Spin–orbit branching in the photofragmentation of HCl

Millard H. Alexander, Brigitte Pouilly, and Thierry Duhoo

Citation: The Journal of Chemical Physics **99**, 1752 (1993); doi: 10.1063/1.465292
View online: http://dx.doi.org/10.1063/1.465292
View Table of Contents: http://scitation.aip.org/content/aip/journal/jcp/99/3?ver=pdfcov
Published by the AIP Publishing

Spin–orbit branching in the photofragmentation of HCl

Millard H. Alexander
Department of Chemistry, The University of Maryland, College Park, Maryland 20742

Brigitte Pouilly and Thierry Duhoo
Laboratoire de Dynamique Moléculaire et Photonique, URA 779, Université des Sciences et Technologies de Lille, 59655 Villeneuve d'Ascq Cedex, France

(Received 8 March 1993; accepted 8 April 1993)

The dynamics of the photofragmentation of HCl and DCl, subsequent to $A\,^1\Pi \leftarrow X\,^1\Sigma^+$ electronic excitation, is treated exactly based on new multireference, configuration-interaction *ab initio* calculations of the relevant electronic potential energy curves and off-diagonal matrix elements. The calculated total cross section agrees well with both earlier calculations and experiment. By contrast, the relative cross sections for formation of the two accessible fine-structure channels [$Cl(^2P_{1/2})$ and $Cl(^2P_{3/2})$] disagree with the most recent experimental results, and, more dramatically, with the results of prior theoretical predictions. Analysis of the redistribution of the photofragment flux, as a function of the H–Cl separation, reveals that the product branching is determined at relatively large HCl distances, considerably beyond the Franck–Condon region, and is governed by the spin–orbit coupling between the initially excited $A\,^1\Pi$ state and the $\Omega=1$ components of the $a\,^3\Pi$ and $1\,^3\Sigma^+$ states.

I. INTRODUCTION

In many photodissociation processes, one (or both) fragments appear in open-shell electronic states. In such processes, more than one electronic potential energy surface will correlate with a given fine-structure level of one (or both) fragments. Although photoexcitation will normally occur to a particular electronic state, as the fragments recoil the photodissociation flux can redistribute among all the accessible potential surfaces. The relative branching ratio into the various fragment fine-structure levels can, in principle, provide valuable information on the manner in which this flux redistribution occurs. The dissociation of a hydrogen halide molecule into $H(^2S)$ and $X(^2P)$ fragments provides a relatively simple prototype for the more complicated case of polyatomic dissociation. Four potential energy curves ($^{1,3}\Sigma^+$ and $^{1,3}\Pi$) correlate with the $H(^2S)X(^2P)$ asymptote as shown in Fig. 1. For the hydrogen halides only the $X\,^1\Sigma^+$ state is bound. Dissociation occurs after excitation from this state to the repulsive $A\,^1\Pi$ state. Branching of the nascent photofragmentation flux among the other electronic states occurs preponderantly at long range, where the definite-Λ electronic states, which are well separated in the molecular region, coalesce and are mixed by the atomic spin–orbit Hamiltonian, which is the dominant term at long range.

The general, time-independent theory of the photodissociation of diatomic molecules into open-shell, atomic fragments has been developed in great detail by Freed and co-workers.[1,2] A particular application to the photodissociation of HCl has been reported by Givertz and Balint-Kurti (GB-K),[3] using a formal development somewhat different from that of Freed and co-workers.[1,2] The calculations of GB-K were based on an earlier determination of the underlying HCl potential curves and electronic transition moments by van Dishoeck, Hemert, and Dalgarno (vDHD).[4] The electronically homologous dissociation of the electronically excited K_2 dimer has been studied by Kleiber *et al.*[5] using semiclassical techniques and by Dubs and Julienne[6] using a fully quantum approach. Freed and co-workers have likewise investigated the photodissocation of the electronically similar CH^+ ion,[7,8] for which the lowest energy dissociation channel is $C^+(^2P)+H$.

There has also been considerable experimental interest in the photodissociation of HCl. A number of laser-based techniques have been used to measure the relative yield of Cl atoms in the ground ($^2P_{3/2}$) and excited ($^2P_{1/2}$) states following photoexcitation at 193 and 157 nm.[9–13] Although some of the experiments appeared to agree quite nicely with the calculated[3] branching ratios, both for HCl and DCl, a recent correction for the relative detection efficiency of the two fine-structure levels has resulted in significantly revised values for these branching ratios.[13] The agreement with theory is now less satisfactory.

The present article reports a new theoretical investigation of photodissociation of HCl. Multireference, configuration-interaction calculations with large atomic orbital basis sets are used to provide the necessary molecular electronic potential curves and nonadiabatic coupling matrix elements. With these we then determine photodissociation cross sections using, as will be discussed in the next section, a recent extension[14–16] of the driven equation approach to photofragmentation, due originally to Band, Freed, and Kouri.[17] In Sec. III, we discuss the Hamiltonian for the HCl molecule, in a Hund's case (a) basis, and the transformation into a Hund's case (e) basis, in which the asymptotic analysis is made. The *ab initio* calculations and results are presented in Sec. IV. After a short discussion of the details of the calculations of the photodissociation cross sections in Sec. V, these and the branching ratio for the two spin–orbit states of the Cl atom are presented and compared with the results of previous calculations[3,4] and experiment[9–13,18] in Sec. VI. In a final section, we discuss briefly how the total photofragmentation

 0021-9606/93/99(3)/1752/13/$6.00

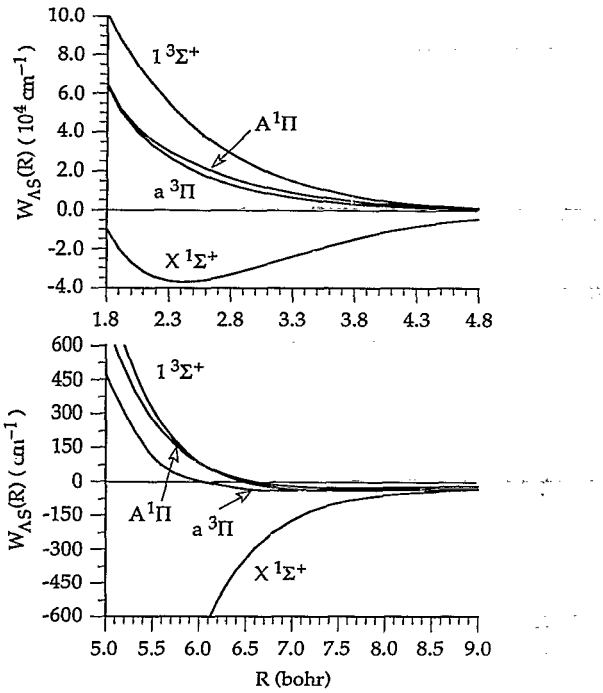

FIG. 1. Potential energy curves for the $X\,^1\Sigma^+$, $A\,^1\Pi$, $a\,^3\Pi$, and $1\,^3\Sigma^+$ states of HCl as determined by the MR-ACPF calculations reported here. The lower panel displays in more detail the long range behavior of the curves.

cross section and the product branching ratio are governed separately by the behavior of the underlying potential curves and coupling matrix elements over different ranges of the photofragment separation.

II. FORMULATION OF THE PHOTODISSOCIATION

Within the driven equations approach of Band, Freed, and Kouri,[17] the photodissociation amplitude can be obtained from the solution $\psi(R)$ to a set of inhomogeneous equations. These are, in matrix notation,

$$\left[\frac{d^2}{dR^2}+W(R)\right]\psi(R)=\chi(R). \tag{1}$$

The column vector $\psi(R)$ represents the coefficients in the expansion of the wave function for the dissociating molecule in terms of the set of electronic states which correlate with the fragment atomic states of interest, namely,

$$\Psi(R)=\frac{1}{R}\sum_n \psi_n(R)\,|\phi_n\rangle. \tag{2}$$

In the present case, $|\phi_n\rangle$ designate the accessible electronic/rotational/fine-structure states of the HCl molecule. In Eq. (1), $W(R)$ designates the $N\times N$ real symmetric wave vector matrix

$$W(R)=k^2-l^2/R^2-(2\mu/\hbar^2)\,[V(R)+H_{so}(R)], \tag{3}$$

where k is the diagonal matrix of asymptotic wave vectors, l is the angular momentum operator for the nuclear orbital motion of the diatom, μ is the collision reduced mass $V(R)$ is the electronic interaction potential, and $H_{so}(R)$ is the spin–orbit Hamiltonian.

Finally, in Eq. (1), $\chi(R)$ is a column vector with elements given by

$$\chi_{nv}(R)=\frac{2\mu}{\hbar^2}\,\mathscr{E}\cdot\mathbf{M}_n(R)\xi_v(R), \tag{4}$$

where $\mathscr{E}$ is the electric field vector of the excitation laser, $\mathbf{M}_n(R)$ is the electronic transition moment between the electronic ground state ($X\,^1\Sigma^+$ for HCl) and the nth electronic excited state, and $\xi_v(R)$ is the wave function of the vth vibrational level of the electronic ground state. The Franck–Condon region is defined as the range of values of R over which $\chi_{nv}(R)$ is significant in size.

Equation (1) is solved subject to the following boundary conditions:

$$\lim_{R\to 0}\psi(R)=0 \tag{5}$$

and

$$\lim_{R\to\infty}\psi(R)=O(R)\tau. \tag{6}$$

Here $O(R)$ is a diagonal matrix with elements proportional to velocity normalized purely outgoing waves. The nth row of the column vector τ represents the amplitude for dissociative excitation into electronic state n of the fragments. Recently, we have described[14–16,19] several algorithms for the determination of the photodissociation amplitude and, subsequently, the photofragmentation wave function. These algorithms are based on the use of log-derivative propagators for the driven equation (1).[14,19–23]

The partial photodissociation cross section, defined as the ratio of the energy absorbed in the transition from the initial bound state wave function into the final photofragment channel n at energy $E=\hbar\omega$ above the energy of the ground state, divided by the incident radiation intensity in the frequency range $\omega\to\omega+d\omega$,[24] is given by

$$\sigma_n(\omega)=\frac{\pi\hbar\omega}{c\epsilon_0\mathscr{E}^2}\,|\tau_n(E)|^2, \tag{7}$$

where ϵ_0 is the permittivity of the vacuum.

III. FRAGMENTATION OF HCl

As discussed briefly in the Introduction, in the molecular region it is most convenient to expand the total scattering wave function in a Hund's case (a) representation.[25–27] The states are labeled by the multiplicity $(2S+1)$, where S is the total electronic spin, by the total angular momentum J, by the quantum numbers Λ and Ω which are the projections along the molecular axis of the electronic orbital angular momentum $\mathbf{L}$ and the total *electronic* angular momentum $\mathbf{J}(\mathbf{J}=\mathbf{L}+\mathbf{S})$, and by the e/f label[28] which designates the parity of the molecular wave function. The e levels have parity $(-1)^J$, and the f levels have parity $-(-1)^J$. In the absence of an external field, there will be no coupling between levels of different J and/or e/f labels. There are six e-labeled states which

TABLE I. Matrix elements of rotational and spin–orbit Hamiltonians in a Hund's case (a) basis.[a,b,c]

	$^3\Sigma_1$	$^3\Pi_0$	$^3\Pi_1$	$^3\Pi_2$	$^1\Sigma_{0e}(^3\Sigma_{0f})$	$^1\Pi_1$
$^3\Sigma_1$	$B[x+L_\perp^2(^3\Sigma^+)]$	$-2B\sqrt{x}L_3^+$	$\sqrt{2}(-2B+\frac{1}{2}A)L_3^+$	$2B(x-2)^{1/2}L_3^+$	0	$-2^{-1/2}AL_3^+$
		$+2B\sqrt{x}L_3^+$			$-2B\sqrt{x}$	
$^3\Pi_0$		$B[x+1+L_\perp^2(^3\Pi)]+\frac{1}{2}A$	$-B\sqrt{2x}$	0	AL_1^+	0
					$(-4B+A)L_3^+$	
$^3\Pi_1$			$B[x+1+L_\perp^2(^3\Pi)]$	$-2B(x-2)^{1/2}$	0	$-A/2$
					$2B(2x)^{1/2}L_3^+$	
$^3\Pi_2$				$B[x-3+L_\perp^2(^3\Pi)]-\frac{1}{2}A$	0	0
$^1\Sigma_{0e}$					$B[x+L_\perp^2(^1\Sigma)]$	$2B\sqrt{2x}L_1^+$
$^3\Sigma_{0f}$					$B[x+2+L_\perp^2(^3\Sigma)]$	0
$^1\Pi_1$						$B[x-1+L_\perp^2(^1\Pi)]$

[a]For further details, see Refs. 25–27 as well as Table II of K. F. Freed, J. Chem. Phys. **45**, 4214 (1966). The present table corrects some typographical errors in the latter reference.

[b]The matrix is symmetrical; for brevity, only the upper triangle is given. We assume the following notation: $x=J(J+1)$; $B=\hbar^2/2\mu R^2$. The matrix elements L_1^+ and L_3^+ are defined by Eqs. (9) and (10). The $L_\perp^2$ matrix elements are defined by $L_\perp^2=\langle^{2S+1}\Lambda|L^2-L_z^2|^{2S+1}\Lambda\rangle$. Finally, A designates the spin–orbit constant of the isolated Cl atom [$A=\frac{2}{3}$ 881 cm^{-1} (Ref. 29)].

[c]When two entries are given, the *upper* entry corresponds to the e labeled states; the lower to the f labeled states.

correlate with the lowest dissociation asymptote of HCl[H(^2S)+Cl(^2P)], namely, $^3\Sigma_1^+$, $^3\Pi_{\Omega=0,1,2}$, $^1\Sigma_0^+$, and $^1\Pi$, and six f-labeled states, namely, $^3\Sigma_1^+$, $^3\Pi_{\Omega=0,1,2}$, $^3\Sigma_0^+$, and $^1\Pi$. If the molecular states are designated $|J\Lambda\Sigma\Omega e/f\rangle$, the matrix elements of the full Hamiltonian in Eq. (1) can be written[27]

$$\frac{\hbar^2}{2\mu}\langle J\Lambda'\Sigma'\Omega' e/f|W|J\Lambda\Sigma\Omega e/f\rangle$$
$$=\delta_{\Lambda\Lambda'}\delta_{\Sigma\Sigma'}\delta_{\Omega\Omega'}[E-W_{\Lambda S}(R)]$$
$$-\langle J\Lambda'\Sigma'\Omega' e/f|H_{so}+B\mathbf{l}^2|J\Lambda\Sigma\Omega e/f\rangle. \quad (8)$$

Here, E is the total energy, $W_{\Lambda S}(R)$ designates the molecular electrostatic potential curves which are assumed to go to zero asymptotically, H_{so} is the spin–orbit Hamiltonian, B is the rotational constant ($B=\hbar^2/2\mu R^2$), and the operator $\mathbf{l}=\mathbf{J}-\mathbf{L}-\mathbf{S}$ describes the relative orbital angular momentum of the nuclei. For reference, Fig. 1 displays the four $W_{\Lambda S}(R)$ potential energy curves for HCl as determined by the *ab initio* calculations which will be described in the next section.

In a simple molecular orbital description of HCl, the nominal electron occupancy for the $^{1,3}\Pi$ states under study here is ... $4\sigma^2 5\sigma^2 6\sigma 1\pi^4 2\pi^3$, which corresponds to H($1s$)Cl(...$3p_\sigma^2 3p_\pi^3$). For the $^{1,3}\Sigma^+$ states, the nominal electron occupancy is ... $4\sigma^2 5\sigma 6\sigma 1\pi^4 2\pi^4$ which corresponds to H($1s$)Cl(...$3p_\sigma 3p_\pi^4$). The presence of a deep well in the $X\,^1\Sigma^+$ state reflects the increasing importance at short range of the electron occupancy ...$4\sigma^2 5\sigma^2 1\pi^4 2\pi^4$ which corresponds to H^+Cl^-(...$3p_\sigma^2 3p_\pi^4$). Within this simple picture, the off-diagonal matrix elements of the electronic orbital angular momentum are given by

$$\langle^1\Pi_{\Lambda=1}|L^+|^1\Sigma_{\Lambda=0}\rangle$$
$$\equiv L_1^+\cong\tfrac{1}{2}[-C_1\langle 2\pi|l^+|5\sigma\rangle+2^{1/2}C_2\langle 2\pi|l^+|6\sigma\rangle], \quad (9)$$

where C_1 and C_2 are the relative weights of, respectively, the covalent (HCl) and ionic terms in the electronic wave function for the $^1\Sigma$ state and

$$\langle^3\Pi_{\Lambda=1,\Sigma=1}|L^+|^3\Sigma_{\Lambda=0,\Sigma=1}\rangle\equiv L_3^+\cong-\tfrac{1}{2}\langle 2\pi|l^+|5\sigma\rangle. \quad (10)$$

The spin–orbit Hamiltonian can be written as[27]

$$H_{so}\cong\sum_i a_i(R)\mathbf{l}_i\cdot\mathbf{s}_i=\sum_i a_i(R)\left[l_{iz}s_{iz}+\frac{1}{2}(l_i^+s_i^-+l_i^-s_i^+)\right], \quad (11)$$

where the spin–other orbit interactions between unpaired electrons have been neglected. At the present time, we do not have the capability to determine the dependence on the HCl separation of the electronic spin–orbit parameter a. As will be discussed later, the product branching ratio in HCl will be governed by the behavior of the potential curves at relatively long range, where the splitting between the curves becomes comparable to the spin–orbit splitting in the Cl atom. In this region, the magnitude of the spin–orbit operator will not be significantly different from its magnitude in the isolated Cl atom [$A=\frac{2}{3}881$ cm^{-1} (Ref. 29)] so that we can write, to a good degree of approximation,

$$H_{so}\cong A\sum_i\left[l_{iz}s_{iz}+\frac{1}{2}(l_i^+s_i^-+l_i^-s_i^+)\right]. \quad (12)$$

Within this approximation and further assuming the validity of the simple molecular orbital picture of the states of HCl introduced earlier in this section, we can express[27] the matrix elements of H_{so} in terms of the spin–orbit constant A and the electronic matrix elements L_1^+ and L_3^+ defined above. Finally, to complete the Hamiltonian in a case (a) basis, we require matrix elements of the operator $L_\perp^2=L^2-L_z^2$. Explicit expressions for the full case (a) Hamiltonian matrix elements for HCl are given in Table I.

At long range, the electronic orbital angular momentum matrix elements can be determined analytically within the "pure precession" limit,[27] namely (in atomic units),

$$\lim_{R\to\infty}L_3^+=\lim_{R\to\infty}L_1^+=-2^{-1/2} \quad (13)$$

and

TABLE II. Transformation between case (e) and case (a) bases for a molecule which fragments into ^2S and ^2P atoms.

			e labeled states [all rows should be divided by $(2J+1)^{1/2}$]					
j	j_{12}	l	$^3\Sigma_1$	$^3\Pi_0$	$^3\Pi_1$	$^3\Pi_2$	$^1\Sigma_0$	$^1\Pi_1$
1/2	1	$J-1$	$-[(J+1)/3]^{1/2}$	$(2J/3)^{1/2}$	$[(J+1)/3]^{1/2}$	0	$-(J/3)^{1/2}$	$-[(J+1)/3]^{1/2}$
1/2	1	$J+1$	$-(J/3)^{1/2}$	$-[2(J+1)/3]^{1/2}$	$(J/3)^{1/2}$	0	$[(J+1)/3]^{1/2}$	$-(J/3)^{1/2}$
3/2	1	$J-1$	$-[(J+1)/6]^{1/2}$	$(J/3)^{1/2}$	$[(J+1)/6]^{1/2}$	0	$(2J/3)^{1/2}$	$[2(J+1)/3]^{1/2}$
3/2	1	$J+1$	$-(J/6)^{1/2}$	$-[(J+1)/3]^{1/2}$	$(J/6)^{1/2}$	0	$-[2(J+1)/3]^{1/2}$	$(2J/3)^{1/2}$
3/2	2	$J-1$	$[(J-1)/2]^{1/2}$	0	$[(J-1)/2]^{1/2}$	$(J+2)^{1/2}$	0	0
3/2	2	$J+1$	$-[(J+2)/2]^{1/2}$	0	$-[(J+2)/2]^{1/2}$	$(J-1)^{1/2}$	0	0
			f labeled states					
j	j_{12}	l	$^3\Sigma_0$	$^3\Sigma_1$	$^3\Pi_0$	$^3\Pi_1$	$^3\Pi_2$	$^1\Pi_1$
1/2	0	J	$-(1/3)^{1/2}$	0	$(2/3)^{1/2}$	0	0	0
1/2	1	J	0	$-(1/3)^{1/2}$	0	$(1/3)^{1/2}$	0	$-(1/3)^{1/2}$
3/2	1	J	0	$-(1/6)^{1/2}$	0	$(1/6)^{1/2}$		$(2/3)^{1/2}$
			{Next row should be divided by $[(2J+1)(2J-1)]^{1/2}$}					
3/2	2	$J-2$	$[J(J-1)]^{1/2}$	$[(J+1)(J-1)]^{1/2}$	$[J(J-1)/2]^{1/2}$	$[(J+1)(J-1)]^{1/2}$	$[(J+1)(J+2)/2]^{1/2}$	0
			{Next row should be divided by $[(2J+3)(2J-1)]^{1/2}$}					
3/2	2	J	$-[2J(J+1)/3]^{1/2}$	$-(3/2)^{1/2}$	$-[J(J+1)/3]^{1/2}$	$-(3/2)^{1/2}$	$[3(J+2)(J-1)]^{1/2}$	0
			{Next row should be divided by $[(2J+1)(2J+3)]^{1/2}$}					
3/2	2	$J+2$	$[(J+1)(J+2)]^{1/2}$	$-[J(J+2)]^{1/2}$	$[(J+1)(J+2)/2]^{1/2}$	$-[J(J+2)]^{1/2}$	$[J(J-1)/2]^{1/2}$	0

$$\lim_{R\to\infty}\left[L_\perp^2\left(^{2S+1}\Sigma^+\right)-L_\perp^2\left(^{2S+1}\Pi\right)\right]=1. \tag{14}$$

At long range, where the splitting between the electrostatic potentials $W_{\Lambda S}(R)$ becomes less than the spin–orbit splitting in the Cl atom fragment [881 cm^{-1} (Ref. 29)], it is more appropriate to use a Hund's case (e) basis to expand the molecular wave function.[30–33] Here the states are labeled by j the total electronic angular momentum of the Cl atom, j_{12} the vector sum of $\mathbf{j}$ and the spin of the hydrogen atom ($\mathbf{j}_{12}=\mathbf{j}+\mathbf{s}_H$), l the orbital angular momentum, J the total angular momentum; and the e/f label. In the case of a system which fragments into ^2S and ^2P atoms, the transformation between the case (e) and case (a) bases is a special case of the general transformation given by Freed and co-workers.[34] After correcting for a normalization error in the latter, we obtain the explicit transformation matrix contained in Table II.

In our treatment of the photodissociation, the $X\,^1\Sigma^+$ state is both the state out of which photoexcitation occurs and the lowest of the manifold of states within which the subsequent fragmentation occurs.

IV. *AB INITIO* CALCULATIONS

Previous *ab initio* studies of both the ground and many of the excited states of HCl have been carried out by Hirst and Guest,[35] vDHD,[4] and, in the same year as the latter study, by Bettendorf, Peyerimhoff, and Buenker.[36] In present study, we are interested only in four HCl potential curves which correlate with the lowest $[H(^2S)+Cl(^2P)]$ asymptote ($X\,^1\Sigma^+$, $A\,^1\Pi$, $a\,^3\Pi$, and $1\,^3\Sigma^+$). We report here new *ab initio* determinations of the potential energy curves for these states, carried out with the augmented correlation-consistent quadruple-zeta (avqz) basis sets of Dunning and co-workers.[37,38] For the H atom, the ($7s4p3d2f$) subset of the primitive basis was contracted as recommended to ($5s4p3d2f$). For the Cl atom, the ($17s12p4d3f2g$) subset of the primitive basis was contracted as recommended to ($7s6p4d3f2g$). This avqz basis included a total of 130 contracted functions.

Using the basis set as described above, complete active space self-consistent field[39] (CASSCF) calculations with 16 electrons in the full space of 6σ and 2π orbitals (with the exclusion of the $1s$ orbital of Cl) were performed. The earlier calculations[4,36] showed that at very short distances the $1\,^3\Sigma^+$ state begins to acquire some Rydberg character, as witnessed by the increasing importance of the electron occupancy $...4\sigma^2 5\sigma 7\sigma 1\pi^4 2\pi^4$ which corresponds to the Rydberg state $H(1s)Cl(...3p_\sigma^0 3p_\pi^4 4s)$. If we include the 7σ orbital in the active space in the CASSCF calculations, we find that it does indeed correspond to a Cl($4s$) orbital at very short distances, in the calculations for triplet multiplicity, but becomes a Cl $3d_z$ orbital at larger R. Since we were reluctant to extend the active space to include all the Cl $3d$ orbitals (which would be necessary for an even-handed description of the contribution of $3d$ orbitals to both the Σ and Π states) and since the contribution of the $4s$ orbital is important only at very small R, we limited the active space to six σ orbitals, assuming that the contribution of the $6\sigma\rightarrow 7\sigma$ excitation could be picked up in the subsequent configuration interaction. In the determination of the electronic matrix elements, state averaging[40–42] was used to obtain a single set of CASSCF orbitals for the Σ and Π states of, separately, singlet and triplet multiplicity. However, a slightly better representation of each state can be obtained by optimizing the CASSCF orbitals separately, for each of the four states. This will be particularly true for the singlet states whenever the ionic H^+Cl^- component of the Σ state is considerable. This latter procedure was followed in the determination of the energies of each state.

Starting with these CASSCF orbitals and wave functions, we then carried out multireference, internally con-

TABLE III. Calculated HCl interaction energies (cm^{-1}).[a]

		$1\,^3\Sigma^+$			
R (bohr)	$X\,^1\Sigma^+$	MR-ACPF	MR-CI(D)[b]	$A\,^1\Pi$	$a\,^3\Pi$
1.1	286 910.0			363 710.0	362 400.0
1.3	134 566.9			210 449.2	209 325.9
1.7	4 093.2			78 586.3	77 683.1
1.75			108 183.0		
1.9	−20 179.4			53 025.5	51 838.0
2.0			78 947.7		
2.1	−31 886.9			38 881.4	36 863.3
2.25			58 529.0		
2.3	−36 344.8			30 097.0	27 038.4
2.4	−36 882.5	47 708.0		26 786.5	23 319.2
2.5	−36 657.5	42 285.7		23 845.8	20 104.3
2.6	−35 866.2	37 367.7		21 163.5	17 351.2
2.8	−33 160.2	28 982.1		16 565.0	12 958.7
3.0	−29 621.4	22 301.3		12 899.4	9 704.9
3.5	−20 080.8	11 292.1		6 757.1	4 743.9
4.0	−12 044.5	4 901.1		3 395.6	2 296.3
4.3	−8 409.8	3 020.5		2 188.4	1 460.6
4.8	−4 292.4	1 278.4		994.9	659.0
5.0	−3 215.5	885.1		708.5	471.9
5.5	−1 518.7	321.3		275.8	111.3
6.0	−709.7	87.2		84.5	4.1
6.5	−340.4	−2.0		7.2	−31.3
7.0	−172.5	−31.1		−19.4	−37.5
8.0	−59.6	−35.8		−23.8	−27.5
8.5	−42.0	−32.4		−20.3	−21.9
9.0	−32.9	−29.2		−16.8	−17.5
10.0	−25.2	−24.6		−11.7	−11.9
11.0	−22.2	−22.1		−9.0	−9.0
12.0	−20.8	−20.8		−7.6	−7.6
15.0	−19.4	−19.4		−6.1	−6.1

[a]All energies determined from MR-ACPF calculations are described in Sec. IV, except as indicated. The CASSCF orbitals in these MR-ACPF calculations were optimized separately for each state.
[b]Multireference CI calculations with Davidson correction.

tracted, configuration-interaction calculations[43] excluding only the 1s electrons of Cl. The reference spaces consisted of 21, 10, 10, and 16 configuration state functions (CSFs) for the $X\,^1\Sigma^+$, $A\,^1\Pi$, $a\,^3\Pi$, and $1\,^3\Sigma^+$ states, respectively. The effect of higher excitations was included in the calculations of the potential curves, but not in the calculation of the electronic matrix elements, by use of the averaged coupled pair functional (ACPF) method of Gadnitz and Ahlrichs.[44] The total number of contracted (uncontracted) configurations was 85 391 (1 152 023) for the $X\,^1\Sigma^+$ state; 84 969 (744 450) for the $A\,^1\Pi$ state, 86 821 (1 241 722) for the $a\,^3\Pi$ state, and 87 138 (1 686 246) for the $1\,^3\Sigma^+$ state. All calculations were carried out with the MOLPRO suite of *ab initio* programs.[45]

The interaction energy can be written as

$$V(R)=E_{\text{H-Cl}}(R)-E_{\text{H}}(R)-E_{\text{Cl}}(R)-\Delta E_{\text{SC}}. \quad (15)$$

Since the fine-structure branching in the dissociation of HCl will be strongly influenced by the behavior of the potential curves at long range, where the splitting is comparable in magnitude to the fine-structure splitting in the Cl atom [881 cm^{-1} (Ref. 29)], it is essential to obtain an accurate representation of the curves in this region. Toward this goal, we include in Eq. (15) the standard counterpoise correction[46] to the calculated interaction energies by subtracting from the calculated energy of the HCl molecule the energies of the atomic fragments determined in the full orbital space of the supermolecule at the same internuclear distance R. Furthermore, in Eq. (15), ΔE_{SC} designates a correction for the remaining size consistency of the MR-ACPF calculations, namely,

$$\Delta E_{\text{SC}}=E_{\text{H-Cl}}(\infty)-E_{\text{H}}(\infty)-E_{\text{Cl}}(\infty). \quad (16)$$

This was found to be -40.8 cm^{-1} for all four states.

The resulting interaction potentials are listed in Table III and displayed in Fig. 1. In the calculations for the $1\,^3\Sigma^+$ state, for distances less than 2.3 bohr, we encountered convergence difficulties in the MR-ACPF calculations, due likely to increasing importance of the 7σ orbital discussed above. Accordingly, for $R<2.4$ bohr, the energies of the $1\,^3\Sigma^+$ state were determined using a multireference, internally contracted CI calculation with the same active space as in the MR-ACPF calculations. The effect of higher order excitations was estimated using the Davidson correction.[47] As can be seen in Table III, the MR-ACPF and MR-CI(D) curves for the $1\,^3\Sigma^+$ state are extremely similar. In the subsequent scattering calculations, the $1\,^3\Sigma^+$ curves were interpolated from the MR-CI(D) values at $R<2.4$ bohr and from the MR-ACPF values at $R\geqslant 2.4$ bohr, smoothly joined in between.

TABLE IV. A comparison of experimental and calculated parameters for the $X\,^1\Sigma^+$ state of HCl.

Method[a]	R_e (Å)	D_e (eV)	ω_e (cm^{-1})	b (cm^{-1} bohr^{-3})[b]
MR-CI	1.285	4.444	2947.8	30 250
MR-ACPF	1.280	4.495	2937.9	31 810
MR-CI[c]	1.275	4.566	2988.8	36 179
MR-ACPF[c]	1.279	4.575	2980.9	35 432
vDHD[d]	1.32	3.9		
	1.29	4.2		
Hirst and Guest[e]	1.288	4.232	3004.9	
Bettendorf *et al.*[f]	1.282	4.34	2961	
Experiment	1.2746[g]	4.6177[g]	2990.95[g]	35 243[h]

[a]See Sec. IV.
[b]Cubic coefficient in expansion of potential. $V(R-R_e)=\frac{1}{2}k(R-R_e)^2-b(R-R_e)^3+\cdots$.
[c]CASSCF orbitals optimized solely for the $X\,^1\Sigma^+$ state. The MR-ACPF parameters are determined from the energies given in Table III.
[d]Calculations of vDHD (Ref. 4); the first entry refers to a calculation with Slater atomic orbitals, the second to a calculation with Gaussian atomic orbitals.
[e]Reference 35.
[f]Reference 36.
[g]Reference 48.
[h]Determined from the Dunham expansion given in Ref. 60.

Table IV presents a comparison between the calculated spectroscopic parameters for the $X\,^1\Sigma^+$ state of HCl and the cubic distortion of the potential curve in the region of the minimum with the results of the earlier calculations of vDHD[4] as well as with the experimental values of these quantities.[48] As anticipated earlier in this section, the best agreement with the experiment is obtained when the CASSCF orbitals are optimized separately for this state. The calculated dissociation energy is only 34 cm^{-1} smaller and the equilibrium internuclear distance, only 0.0045 Å larger than the experimental values. If the calculated MR-ACPF $X\,^1\Sigma^+$ potentials are shifted to smaller R, to correct for the slight inaccuracy in the calculated value of R_e, and the origin taken as the bottom of the well, the calculated curves are virtually *indistinguishable* from the experimentally derived potential curve of Ogilvie and Koo.[49]

The vertical excitation energies from the $X\,^1\Sigma^+$ state at $R=2.4$ (close to the calculated minimum) to the $a\,^3\Pi$ and $A\,^1\Pi$ states are, respectively, 60 200 and 63 670 cm^{-1}, which are slightly larger than the comparable values of Bettendorf *et al.*,[36] namely, 59 603 and 63 223.

The upper panel of Fig. 2 shows the dependence on the HCl bond distance R of the $A\,^1\Pi$–$X\,^1\Sigma^+$ electronic transition moment defined as[50]

$$M_{\Sigma\Pi}(R)=-2^{-1/2}e\langle A\,^1\Pi_{\Lambda=1}|x+iy|X\,^1\Sigma^+\rangle$$
$$=-e\langle A\,^1\Pi_x|x|X\,^1\Sigma^+\rangle, \qquad (17)$$

where e is the electronic charge. The definition of the transition moment used by Van Dishoeck and co-workers[4] (and, presumably, also by GB-K,[3] although the latter do not explicitly give a definition)

$$M_{\Sigma\Pi}(R)=-2^{-1/2}e\langle A\,^1\Pi_{e/f}|x+iy|X\,^1\Sigma^+\rangle, \qquad (18)$$

is $\sqrt{2}$ *larger* in magnitude than the accepted[50] definition of the transition moment given in Eq. (17). After compensation for this difference, our transition dipole moment is compared, also in the upper panel of Fig. 2, with the transition dipole moment functions reported by vDHD[4] and that used by GB-K[3] to obtain a best fit of the experimentally available total dissociation cross section for HCl, from calculations based on the earlier *ab initio* work of vDHD. The present calculations yield a transition dipole moment which resembles the earlier transition moments, particularly over the classically allowed range of motion in the lowest vibrational level of the X state of HCl, but is somewhat smaller than the transition moment of vDHD. The classical turning points of the $v=0$ vibrational level of the $X\,^1\Sigma^+$ state, as predicted by our MR-ACPF calculations, are 2.23 and 2.66 bohr. This range of internuclear separation defines the Franck–Condon region over which the major fraction of the excitation to the $A\,^1\Pi$ state will occur.

The lower two panels of Fig. 2 display the dependence on R of the $\langle A\,^1\Pi|L^+|X\,^1\Sigma^+\rangle$ and $\langle a\,^3\Pi|L^+|1\,^3\Sigma^+\rangle$ electronic coupling matrix elements and the difference be-

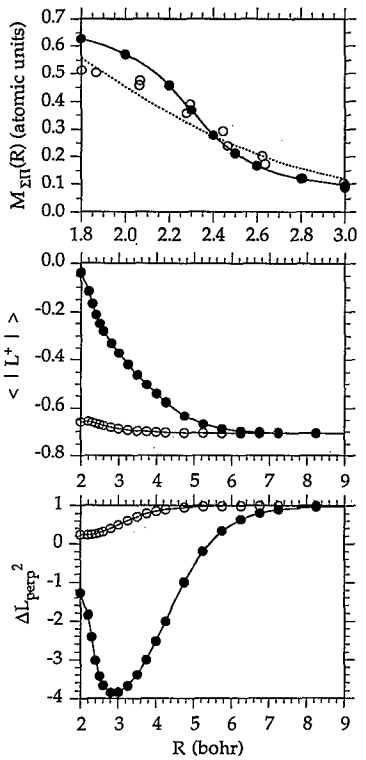

FIG. 2. (Upper panel) The $A\,^1\Pi$–$X\,^1\Sigma^+$ electronic transition moment, as a function of the HCl bond distance, as predicted by the MR-CI calculations reported here. For comparison, the dashed curve depicts the dipole moment function used by GB-K (Ref. 3) and the open circles indicate the results of the earlier *ab initio* calculations of vDHD (Ref. 4). The numerical values given by these authors have been multiplied by $2^{-1/2}$ to conform to the recommended definition of the electronic transition moment [Ref. 50, Eq. (17)]. (Middle panel) Dependence on the HCl bond distance of the electronic matrix elements $\langle A\,^1\Pi|L^+|X\,^1\Sigma^+\rangle$ (filled circles) and $\langle a\,^3\Pi|L^+|1\,^3\Sigma^+\rangle$ (open circles). In the pure-precession limit (Refs. 25 and 27), both these matrix elements are equal to $-2^{-1/2}$. (Lower panel) Dependence on R of the difference between the diagonal matrix elements $\langle X\,^1\Sigma^+|L_\perp^2|X\,^1\Sigma^+\rangle$ and $\langle A\,^1\Pi|L_\perp^2|A\,^1\Pi\rangle$ (filled circles) and the difference between the $\langle 1\,^3\Sigma^+|L_\perp^2|1\,^3\Sigma^+\rangle$ and $\langle a\,^3\Pi|L_\perp^2|a\,^3\Pi\rangle$ matrix elements (open circles). In the pure-precession limit, both these differences are equal to 1.

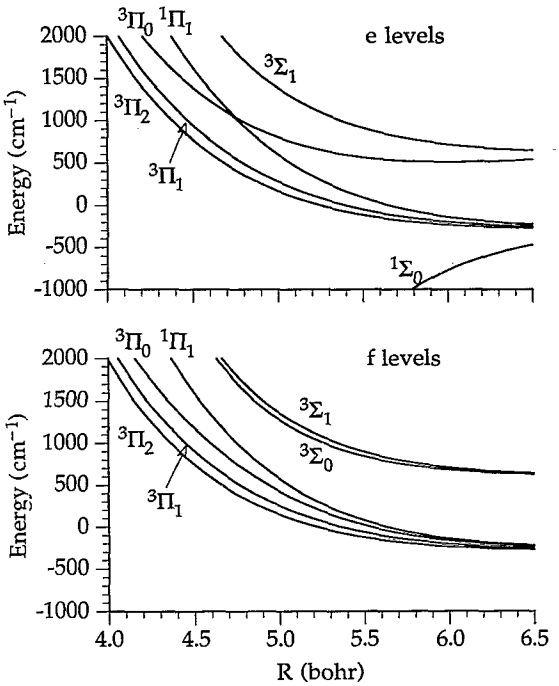

FIG. 3. Adiabatic potential curves for $J=2$ for the e states (upper panel) and f states (lower panel) in the region where the transformation from case (a) to case (e) occurs. The nominal case (a) labeling is indicated. The crossing between the $^1\Pi_1$ and $^3\Pi_0$ e-labeled curves is only weakly avoided, since there is no direct coupling between these two states (Table I).

tween the diagonal matrix elements of $L_\perp^2$ (Table I).[51] We observe that the pure precession limit applies well to HCl, particularly for the triplet states. For the singlet state, the increasing admixture of H^+Cl^- ionic character into the wave function results in a more pronounced quenching of the L^+ matrix element at shorter distances.

In the discussion of photodissociation[1,5,6,14,15,52,53] processes, it is useful to expand the wave function in a *fully adiabatic* basis

$$\phi^a(R)=T(R)\phi(r), \tag{19}$$

where $T(R)$ is the matrix which continuously diagonalizes the $W(R)$ matrix at each value of R. We have

$$TW(R)T^T=(\hbar^2/2\mu)\lambda(R), \tag{20}$$

with $\lambda(R)$ designating the diagonal matrix of adiabatic energies. For simplicity, in Eq. (19) we have dropped the state label n of Eq. (2).

Figure 3 illustrates the behavior of the fully adiabatic energies for both the e and f levels for $J=2$. For the f-labeled states, the nominal $A\,^1\Pi$ state correlates adiabatically with the lower ($^2P_{3/2}$) Cl spin–orbit state. For the e-labeled state, the nominal $A\,^1\Pi$ state undergoes an avoided crossing with the $a\,^3\Pi_0$ state. This crossing is only weakly avoided because there is no direct coupling between a $^1\Pi$ and a $^3\Pi_0$ state (Table I). Hence we would anticipate, from adiabatic correlation arguments, that photodissociation of HCl via the unbound $A\,^1\Pi$ state would lead predominantly to Cl atoms in the lower ($^2P_{3/2}$) spin–orbit state.

V. PHOTODISSOCIATION CALCULATIONS

With the calculated *ab initio* potentials and nonadiabatic matrix elements, and explicitly assuming that the magnitude of the spin–orbit constant A in Table I remains equal to its asymptotic value (587 cm^{-1}), we have solved Eq. (1) to obtain the photodissociation cross sections. In the determination of the solution to Eq. (1), the propagation was carried out in the case (a) basis using the Hamiltonian of Table I. Asymptotically, the solution was transformed to the asymptotically diagonal case (e) basis before determination of the photofragmentation amplitudes. All scattering calculations were carried out with our Hibridon code.[54]

In our treatment of the photodissociation, the $X\,^1\Sigma^+$ state is both the state out of which photoexcitation occurs and the lowest of the manifold of states within which the subsequent fragmentation occurs. For excitation out of the $v=0$ level of the $X\,^1\Sigma^+$ state, the vibrational wave function [$\xi_v(R)$ in Eq. (4)] was taken to be the lowest wave function for a Morse oscillator with parameters (in atomic units) $D_e=0.168\,11$, $R_e=2.4154$; $\beta=0.994\,71$, which resulted from a fit of the *ab initio* MR-CPF curve for the $X\,^1\Sigma^+$ state in the vicinity of R_e. This is virtually identical to the exact (numerically integrated) ground state vibrational wave function. Givertz and Balint-Kurti[3] have argued that, in addition to the $A\,^1\Pi$–$X\,^1\Sigma^+$ transition moment, one must also take into account the $a\,^3\Pi$–$1\,^3\Sigma^+$ moment, due to the presence of a significant degree of triplet character in the ground electronic state, induced by spin–orbit coupling (Table I). However, with our calculated potential energy curves, diagonalization of the case (a) Hamiltonian revealed that the largest admixture of triplet character (that of the $^3\Pi_0$ state) was negligibly small ($<0.5\%$ within the Franck–Condon region).

For a given initial $J''M''$ rotational level of the HCl molecule in its $X\,^1\Sigma^+$ state, photoexcitation to the $A\,^1\Pi$ state at frequency ω will populate e parity levels by either P or R branch excitation with $J'=J''\mp1$, respectively, or f parity levels by Q branch excitation with $J'=J''$. We can add explicitly the initial and final rotational and projection quantum numbers to the notation for the photodissociation cross section of Eq. (7) to write $\sigma_n(J''M''\rightarrow J'M',\omega,\mathscr{E})$. In the calculation of this cross section, we must use the transition dipole appropriate to a $^1\Pi\leftarrow{}^1\Sigma^+$ transition from rotational level $J''M''$ to rotational level $J'M'$ with the electric field direction given by $\mathscr{E}$. For an isotropic distribution of molecules, the effective photodissociation cross section out of initial rotational level J'' can be obtained by summing over all final rotational quantum number and averaging over initial projection states, namely,

$$\sigma_n(\omega,\mathscr{E})=(2J''+1)^{-1}\sum_{J',M',M''}\sigma_n(J''M''\rightarrow J'M',\omega,\mathscr{E}), \tag{21}$$

where the sum extends over values of J' consistent with all three spectroscopic branches.

The present calculations showed that, for a given transition dipole moment, the state resolved photodissociation cross sections were virtually identical for all three allowed final rotational quantum numbers ($J'=J''$, $J''\pm1$) and *independent* of the e/f label. In this case, the explicit expressions for the rotational line strength factors[25,55] for a $^1\Pi\leftarrow{}^1\Sigma^+$ transition can be used to show that the effective photodissociation cross section is equal to 4/3 of the cross section given by Eq. (7), calculated for a particular (e or f) parity using a transition dipole moment of magnitude equal to the purely electronic transition moment of Eq. (17). This factor of 4/3 is consistent with that used in earlier work on molecular photodissociation[56,57] and assumes a definite direction for the electric field vector $\mathscr{E}$ of the excitation light source. Summing over all possible directions of $\mathscr{E}$, as is conventional in the definition of spectroscopic line strength factors,[50,58] would result in multiplication by an additional factor of 3. This was *not* done in the results to be presented here.

In addition to the total photodissociation cross section, an important experimentally accessible parameter is the branching ratio between the two fine-structure levels ($j=1/2$, $3/2$) of the Cl atom. This ratio is defined as the photodissociation cross section summed over the two $j=1/2$ case (e) levels divided by the photodissociation cross section summed over the four $j=3/2$ case (e) levels. In a purely statistical limit, this ratio will equal 1/2, the ratio of the rotational degeneracies of the two fine-structure levels. Deviations from this statistical limit shed light on the redistribution of the photodissociation flux, as the system crosses from the molecular region, where a Hund's case (a) description is appropriate, into the asymptotic region, where a Hund's case (e) description is suitable. By contrast, as discussed at the end of Sec. IV, adiabatic correlation arguments would predict a branching ratio of zero.

VI. COMPARISON WITH EARLIER CALCULATIONS AND EXPERIMENT

Givertz and Balint-Kurti[3] considered a somewhat simplified model for the photodissociation of HCl, treating excitation out of the $J=0$ rotational level of the $X\,^1\Sigma^+$ ground state into just the $\Omega=1$ projection states of the $J=1$ level. They neglected all off-diagonal rotational coupling terms (the off-diagonal terms in Table I which depend on the rotational constant B) and further assumed that the spin–orbit constant was independent of R. We too made this latter approximation. Although GB-K did not take use parity adapted basis functions (which allows one to block diagonalize the Hamiltonian into e and f states), they reduced the dimensionality of the close coupled expansion by restricting themselves to just the $\Omega=1$ projection states of the $J=1$ level ($^3\Pi_{1e}+{}^3\Pi_{1f}$, $^3\Sigma_{1e}+{}^3\Sigma_{1f}$, and $^1\Pi_{1e}+{}^1\Pi_{1f}$) and the four possible case (a) states for $J=0$ ($^1\Sigma_0$, $^3\Pi_{0e}\pm{}^3\Pi_{0f}$, and $^3\Sigma_{0f}$). As can be seen in Table I, this block diagonalization of the Hamiltonian is justified, if one neglects all off-diagonal rotational coupling terms.

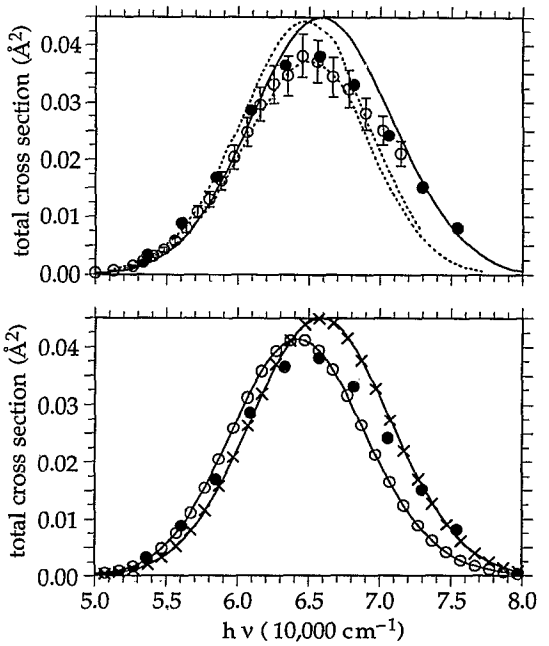

FIG. 4. (Upper panel) Total cross section for $A\leftarrow X$ dissociation out of the $v=0$ level of the HCl molecule as a function of photon energy. The solid curve refers to a total angular momentum of $J=2$. For comparison, the filled circles indicate the earlier predictions of GB-K (Ref. 3) and the open circles indicate the experimental values of Inn (Ref. 18) with error bars of $\pm10\%$, as recommended therein. The dashed curves indicate the range of cross sections predicted by vDHD (Ref. 4). (Lower panel) A comparison of total cross sections determined by the present *ab initio* calculations (solid curves) with the results ($\times$'s) of equivalent calculations, but neglecting all rotational coupling matrix elements in the Hamiltonian [Eqs. (13) and (14)]. In addition, the open circles represent cross sections determined with the full molecular Hamiltonian (Table I), but using the $A\,^1\Pi$–$X\,^1\Sigma^+$ transition electric dipole moment function of GB-K (Ref. 3), while the filled circles, as in the upper panel, indicate the earlier predictions of the latter authors.

The upper panel of Fig. 4 displays the calculated photodissociation cross sections for $J=2$ and excitation of the $^1\Pi$ state. Comparison calculations at several energies indicated that the calculated cross sections were virtually identical for excitation of the e or f levels and displayed an almost negligible variation with the total angular momentum. The curves shown represent the sum over all six final states of the partial cross sections given by Eq. (7), further divided by a factor of 2π, so that the displayed cross sections refer to a unit incident radiation intensity over the frequency range $\nu\rightarrow\nu+d\nu$. Also displayed are the total photodissociation cross sections from the earlier calculations of vDHD[4,59] and GB-K[3] and the experimental values of Inn.[18] Our calculated cross sections agree well with the previous values, both in the position of the maximum absorption and the width of the absorption profile. In the region of the maximum, the calculated cross sections lie slightly outside of the experimental error bars.

To ensure the visibly excellent agreement with experiment, GB-K adjusted the $X\rightarrow A$ transition dipole moment function as well as the functional form of the A state potential curve. As is illustrated in the upper panel of Fig. 3, the transition dipole function used by GB-K differs in

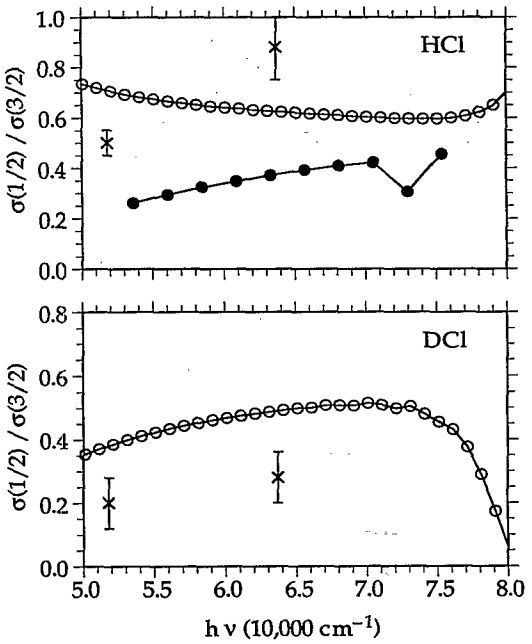

FIG. 5. (Upper panel) Predicted Cl atom branching ratio $[\sigma(j=1/2)/\sigma(j=3/2)]$ in the photofragmentation of HCl ($v=0$) as a function of collision energy at a total angular momentum of $J=2$ (open circles). The filled circles indicate the earlier predictions of GB-K. The experimental values and error bars are taken from Refs. 9, 12, and 13. (Lower panel) An equivalent graph, but for the DCl isotope. The experimental values and error bars are taken from Ref. 13.

shape from the *ab initio* function. To explore the sensitivity of the photodissociation cross sections on the X–A transition dipole, we repeated our present calculations with the dipole moment function of GB-K.[3] The resulting cross sections are displayed in the lower panel of Fig. 4. We observe a noticeable difference in the frequency dependence of the photodissociation cross section. Since the modified results are based on the transition dipole moment of GB-K and the present *ab initio* potentials, they also differ from the earlier predictions of GB-K,[3] which were based on their transition moment and the potential curves of vDHD.[4]

The lower panel of Fig. 4 also compares ($\times$'s) the photodissociation cross sections calculated under the neglect of all rotational coupling terms in the Hund's case (a) molecular Hamiltonian (Table I). As discussed at the beginning of this section, this was the dynamical approximation made by GB-K.[3] It is clear from the lower panel of Fig. 4 that neglect of these terms has *no effect* on the photodissociation cross section. As might then be anticipated, the calculated photodissociation cross section is also unaffected (not shown) by the replacement of the exact values of the diagonal and off-diagonal rotational coupling matrix elements by values appropriate to the pure-precession limit.

Figure 5 displays the calculated branching ratios for both HCl and DCl as a function of the excitation energy. Also shown are the predictions of GB-K[3] and the available experimental data for photoexcitation at wavelengths of 157 and 192 nm.[9–13] The quantitative comparison with experiment is given in Table V. We observe considerable disagreement, both in magnitude and energy dependence, between our results and the experimental branching ratios as well as those calculated by GB-K.[3] Our calculations predict a smaller tendency for population of the upper spin–orbit state, in the case of DCl, which is also in agreement with experiment. Simple semiclassical considerations might also predict that at low energy, the photodissociation flux would tend to evolve *adiabatically*. From the adiabatic curves shown in Fig. 3, we see that this would imply a strong propensity toward population of the lower ($j=3/2$) multiplet levels. As the energy increases, the tendency toward nonadiabaticity would also increase, as seen in the calculated results. At higher energies, in the high frequency tail of the absorption profile (Fig. 4), there appears to be a dramatic drop in the DCl branching ratios.

By contrast, in the case of HCl, the tendency toward adiabaticity actually *increases* with increasing energy, in contrast to both the experimental results and the predictions of GB-K.[3] Notwithstanding the noticeable variation with excitation frequency, to a first approximation, the fine

TABLE V. Product branching ratios $[\sigma(j=1/2)/\sigma(j=3/2)]$ in the photodissociation of HCl ($v=0$) and DCl ($v=0$).

		HCl		DCl	
Determination	J	193 nm	157 nm	193 nm	157 nm
ab initio[a]	10	0.66	0.59	0.28	0.45
	2	0.64	0.58	0.28	0.44
GB-K $M_{\Sigma\Pi}$[b]	2	0.64	0.57		
GB-K[c,d]	1	0.24	0.37		<0.20
Experiment		0.50±0.05[e,f,g]	0.88±0.13[e]	0.20±0.08[e]	0.28±0.08[e]

[a]Present calculations. The branching ratios for $J=1$ are identical to those for $J=2$.
[b]Present formulation, but using the dipole moment function of Ref. 3.
[c]Reference 3.
[d]Values taken from Ref. 11.
[e]Reference 13.
[f]Reference 9.
[g]Reference 12.

structure branching ratios, for both isotopes, lie close to the statistical limit of 1/2.

Although, as shown by the lower panel of Fig. 4, there were notable differences between the total photodissociation cross sections determined with our *ab initio* transition dipole moment function and the dipole moment function of GB-K, the predicted branching ratios are almost identical. Similarly, and also not shown in Fig. 5, replacement of the rotational coupling matrix elements by their pure precession limits and, more dramatically, the neglect of these matrix elements altogether, have a *negligible* effect on the predicted branching ratios.

VII. DISCUSSION

Within the Franck–Condon region ($2.23 \leqslant R \leqslant 2.66$ bohr), there is little non-Born–Oppenheimer mixing of the $X\,^1\Sigma^+$ or the $A\,^1\Pi$ state with the triplet states. Thus the extent of photoexcitation to the unbound A state and, consequently, the *total* photodissociation cross section, is little affected by these other states. It is for this reason that our predicted total cross section, as a function of excitation frequency, is independent of the e/f label (parity) of the excited A state level and also virtually unaffected if the non-Born–Oppenheimer coupling to the triplet states is approximated by the pure-precession limit, or more drastically, if the rotationally coupling is neglected entirely. The unimportance of the triplet states in the description of the photoexcitation is further confirmed by the good overall agreement between our calculations and the previous calculations of vDHD[4] and GB-K,[3] who used a considerably simplified description of the coupling between the X and A states and the neighboring triplet states.

Thus the photoexcitation can be treated as a two-state process involving only the potential curves of the $X\,^1\Sigma^+$ and the $A\,^1\Pi$ states, and *independent* of the electronic symmetry of the latter. As seen in Fig. 4, the total photodissociation cross section will be sensitive only to the shape of the A state potential curve, and the magnitude and shape of the X–A transition dipole in the Franck–Condon region.

On the other hand, the branching between the two fine-structure levels of the Cl atom photofragment will be governed by the non-Born–Oppenheimer coupling between the initially excited $A\,^1\Pi$ state and the neighboring triplet states in the region where these coalesce and then separate onto the two Hund's case (e) asymptotes. As can be seen in Fig. 3, this occurs over the range $4 \leqslant R \leqslant 6$ bohr, well outside the Franck–Condon region. Since the product branching ratio was found to be unchanged if all the rotational coupling terms in the Hamiltonian were neglected (Table I), this ratio must be governed only by the magnitude of the spin–orbit coupling term in the Hamiltonian and, of course, by the shape of the molecular potentials over the range $4 \leqslant R \leqslant 6$ bohr. As can be seen in Table I, the spin–orbit Hamiltonian couples the initially excited $A\,^1\Pi$ state only with the $\Omega=1$ components of the triplet states. In the case of the f labeled states, the $A\,^1\Pi$ state correlates with the lower spin–orbit state of the fragments (lower panel of Fig. 3). Since the product branching ratio was found to be virtually independent of the e/f label of the initially excited state, we can also assert that this correlation [$A\,^1\Pi \rightarrow \mathrm{Cl}(^2P_{3/2})$] will be virtually unaffected by the weak avoided crossing between the $^1\Pi_1$ and $^3\Pi_0$ e-labeled curve seen in the upper panel of Fig. 3.

Thus the formation of photofragments corresponding to the upper [$\mathrm{Cl}(^2P_{1/2})$] spin–orbit channel will be governed principally by the degree to which photofragment flux is removed from the initially excited $A\,^1\Pi$ state by the spin–orbit coupling with the $\Omega=1$ component of the $1\,^3\Sigma^+$ state, which correlates with the $\mathrm{Cl}(^2P_{1/2})$ asymptote. Since there is no direct coupling between the $A\,^1\Pi$ state and the $\Omega=0$ component of the $1\,^3\Sigma^+$ state, the presence of the $^3\Sigma_0^+$ curve in the f-labeled states (lower panel of Fig. 3) will have little effect on the product branching.

Since our calculated branching ratios were only slightly affected when the *ab initio* transition dipole moment function was replaced with the phenomenological dipole moment function of GB-K,[3] and since the branching ratios are insensitive to the inclusion of rotational coupling, at least for low to moderate values of J, the sizable difference between our predicted branching ratios and those predicted by GB-K[3] likely reflect differences in the behavior of the H–Cl potential curves in the region ($4 \leqslant R \leqslant 6$ bohr).

A significantly smaller product branching ratio into the upper spin–orbit state is predicted for DCl as compared to HCl, although the potential curves and off-diagonal spin–orbit couplings are *identical*. This can be explained by a reduced tendency for the system with heavier reduced mass to undergo nonadiabatic transitions, especially at lower values of the excitation frequency, where the relative velocity of the nascent fragments will be smaller.

In several recent papers,[14,15,53] we have demonstrated how the current density associated with the solution $\psi(R)$ to Eq. (1) provides a means to investigate the dependence of the photodissociation process on the interfragment separation. Flux rises in the various channels of the unbound excited state as the initially bound fragments move through the region where the photon is absorbed, and then is redistributed because of interactions in the excited state. The total photofragment flux at an interparticle separation R,$J(R)$, is the sum of photofragment fluxes associated with each internal state n, namely,[14,15,53]

$$J(R) = \sum_n J_n(R), \tag{22}$$

where

$$J_n(R) = \frac{\hbar}{\mu} \mathrm{Im}[\psi_n(R)^* \psi_n'(R)]. \tag{23}$$

At large interparticle separations, these channel fluxes become equal to the squares of the photodissociation amplitudes which appear in Eq. (7)[14,15,53]

$$J_n(R \rightarrow \infty) = |\tau_n|^2. \tag{24}$$

Figure 6 illustrates the dependence on the H–Cl distance R of the photofragment flux subsequent to Q branch absorption by a HCl molecule with $J=2$ of a photon of wavelength 157 nm. The upper panel traces the evolution of the flux in the fully adiabatic basis [Eq. (19), Fig. 3] as

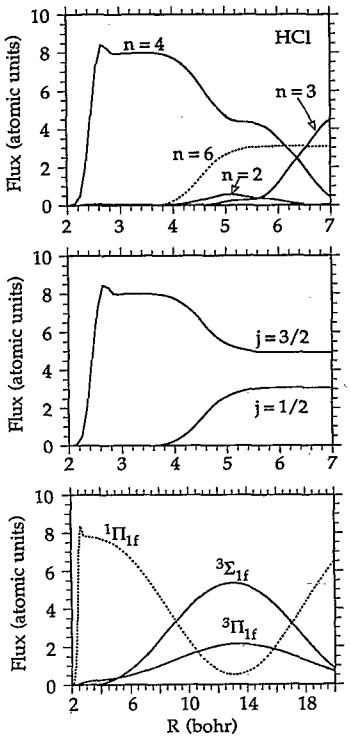

FIG. 6. (Upper panel) Dependence on the H–Cl internuclear distance of the photofragment flux associated with the f parity adiabatic states with $J=2$ (Fig. 3) subsequent to absorption of a photon of wavelength 157 nm. There is no perceptible distribution of flux into the $n=1$ or $n=5$ states. (Middle panel) A similar plot in which the displayed photofragment fluxes represent the sum of the fluxes associated with the two adiabatic states ($n=5$ and 6) which correlate asymptotically with the $j=1/2$ fine-structure level of Cl (lower curve), and the four adiabatic states ($n=1$–4) which correlate asymptotically with the $j=3/2$ fine-structure level. (Lower panel) A similar plot illustrating the redistribution of the photofragment flux, but in terms of the Hund's case (a) molecular states. The redistribution of flux into the $^3\Sigma_0$, $^3\Pi_0$, or $^3\Pi_2$ states is negligibly small.

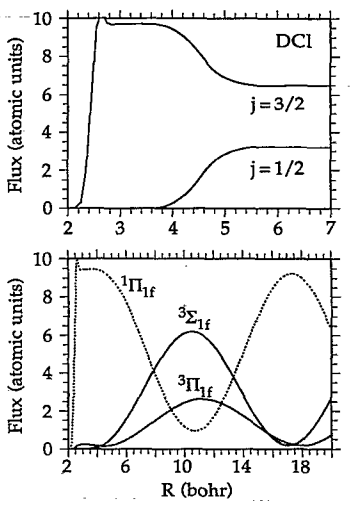

FIG. 7. (Upper panel) Dependence on the D–Cl internuclear distance of the photofragment flux associated with the f parity adiabatic states with $J=2$ (Fig. 3) subsequent to absorption of a photon of wavelength 157 nm. The displayed photofragment fluxes represent the sum of the fluxes associated with the two adiabatic states ($n=5$ and 6) which correlate asymptotically with the $j=1/2$ fine-structure level of Cl (lower curve), and the four adiabatic states ($n=1$–4) which correlate asymptotically with the $j=3/2$ fine-structure level. (Lower panel) a similar plot illustrating the redistribution of the photofragment flux, but in terms of the Hund's case (a) molecular states. The redistribution of flux into the $^3\Sigma_0$, $^3\Pi_0$, or $^3\Pi_2$ states is negligibly small.

a function of R. Flux appears initially in the $n=4$ state, which corresponds, in the molecular region, to the $^1\Pi_{1f}$ state. The flux remains exclusively in this state from the outer edge of the Franck–Condon region ($R=2.7$ bohr) until $R\cong 4$ bohr, at which point, flux begins to appear in the $n=6$ state, which corresponds to the $^3\Sigma_{1f}$ state. At larger distances, the flux associated with this state, which correlates with the upper ($j=1/2$) spin–orbit level of the Cl atom (Fig. 3), remains constant. On the other hand, at larger distances, we observe considerable redistribution of flux associated with the adiabatic levels ($n=1$–4) which correlate with the lower ($j=3/2$) spin–orbit level of Cl.

To show that this latter redistribution will not affect the spin–orbit branching ratio, we display in the middle panel of Fig. 6 the fluxes summed over the two adiabatic states ($n=5$ and 6) which correlate with the upper spin–orbit channel and, separately, summed over the four adiabatic states ($n=1$–4) which correlate with the lower spin–orbit channel. This figure reveals how the spin–orbit branching occurs over a relatively broad, but confined range of internuclear separation, well outside of the Franck–Condon region.

In the lower panel, the flux redistribution is displayed in the molecular [Hund's case (a) basis]. Flux appears initially in the $^1\Pi_{1f}$ state, but also, to a much smaller extent, in the $^3\Pi_{1f}$ state. The appearance of flux in the latter state reflects the near degeneracy of the $^1\Pi$ and $^3\Pi$ potential curves at short range (Fig. 1) and the presence of spin–orbit coupling between these two states (Table I). At longer range, flux is increasingly transferred out of the $^1\Pi$ state into both the $^3\Pi_{1f}$ and $^3\Sigma_{1f}$ states, both of which are spin–orbit coupled to the $^1\Pi_{1f}$ state. As R increases, the rotational coupling terms, which vary as R^{-2} become negligibly small, and the flux flows in an oscillatory manner among these three states. Since the off-diagonal spin–orbit coupling is *independent* of R, at least in the pure-precession limit, the dependence of R of this oscillatory flux transfer displays a regular periodicity.

Figure 7 illustrates the flux redistribution which accompanies the fragmentation of DCl, again for Q-branch excitation of the f levels with $J=2$ at a wavelength of 157 nm. Comparing the upper panel of Fig. 7 with the middle panel of Fig. 6, we observe a great degree of qualitative similarity in the dissociation of the HCl and DCl isotopes. In particular, the curves which describe the rise in flux associated with the upper two ($n=5$ and 6) adiabatic states are almost *identical* for the two isotopes. Since, however, the initial photoexcitation is slightly more efficient in the case of DCl at the particular wavelength chosen, the *relative* degree of flux transfer out of the initially populated $n=4$ level into the is slightly less.

The lower panel of Fig. 7 displays the redistribution of the DCl photofragment flux in the molecular basis. Com-

parison of this panel with the lowest panel of Fig. 6 reveals a similar oscillatory structure, but with a shorter wavelength. Since the reduced mass of DCl is almost twice that of HCl for a given energy, the relative fragment recoil velocity will be roughly $\sqrt{2}$ times *slower* in the case of DCl. Consequently, since the strength of the spin–orbit coupling is the same for both isotopes, the beat wavelength will be shorter in the case of DCl, by roughly the same factor of $\sqrt{2}$.

The flux redistribution plots confirm the prediction, made at the beginning of this section, that the spin–orbit branching in the fragmentation of HCl following $A \leftarrow X$ excitation is governed by the behavior of the HCl potentials at relatively long range, considerably outside the Franck–Condon region. In particular, it is the coupling between the initially excited $A\ ^1\Pi$ state and the repulsive triplet states ($a\ ^3\Pi$ and $1\ ^3\Sigma^+$) which is critical. By contrast, the behavior of the potential curve for the attractive $X\ ^1\Sigma^+$ state will have little influence.

It would be interesting to extend the present calculations, particularly the analysis of the redistribution of the photofragment flux, to the investigation of the photofragmentation of other diatomic molecules which correlate to a ^2S and a ^2P atom as, e.g., the excited states of K_2 or NaK, or the molecular ions CH^+ or SiH^+. Although the Hamiltonian matrix will be identical, the relative topology of the potential curves, as well as the energy ordering of the two fine-structure levels, will be different. However, it is likely that in these other cases, as in the case of HCl investigated here, the product branching ratio will be established only at relatively long range at distances where the splitting between the molecular Hund's case (a) potential curves becomes comparable to the spin–orbit splitting in the atom. This distance will be proportionally larger, the smaller the spin–orbit splitting in the ^2P atomic product.

Although our predicted spin–orbit branching ratios for the photodissociation of HCl differ significantly from the earlier predictions of GB-K,[3] there persists a sizable disagreement with the experimental measurements[9–13] at both published excitation wavelengths (193 and 157 nm), even after a recent revision of some of these values.[12,13] In particular, in the case of HCl, the energy dependence of the experimental branching ratios (both in magnitude and slope) differ dramatically from our predictions. The quality of the *ab initio* potential curves (at least for the $X\ ^1\Sigma^+$ state where a comparison with the experimentally derived potential is possible) and the demonstrated insensitivity of the calculated branching ratios to the deviation of the electronic coupling matrix elements from the pure precession limit lend credence to the calculated spin–orbit branching ratios. We are hopeful that future experimental work will provide additional values of this branching ratio over a wider range of energies.

ACKNOWLEDGMENTS

Millard Alexander is grateful to the U.S. Army Research Office for partial support of this work under Contract No. DAAL03-91-G-0129 and to the Université de Lille for a Visiting Professorship without which the research reported here would not have been initiated. He also wishes to thank Hans-Joachim Werner for his invaluable technical advice about the *ab initio* calculations reported here, Gabriel Balint-Kurti for communication of the $A\ ^1\Pi$–$X\ ^1\Sigma^+$ dipole moment function displayed in Fig. 2, and Robert Gordon and George Flynn for illuminating discussions concerning the ongoing experimental study of the photodissociation of HCl.

[1] S. J. Singer, K. F. Freed, and Y. B. Band, Adv. Chem. Phys. **61**, 1 (1985).
[2] C. J. Williams, K. F. Freed, S. J. Singer, and Y. B. Band, Faraday Discuss. Chem. Soc. **82**, 51 (1986).
[3] S. C. Givertz and G. G. Balint-Kurti, J. Chem. Soc. Faraday Trans. **82**, 1231 (1986).
[4] E. F. van Dishoeck, M. C. van Hemert, and A. Dalgarno, J. Chem. Phys. **77**, 3693 (1982).
[5] P. D. Kleiber, J.-X. Wang, K. M. Sando, V. Zafiropulos, and W. C. Stwalley, J. Chem. Phys. **95**, 4168 (1991).
[6] R. L. Dubs and P. S. Julienne, J. Chem. Phys. **95**, 4177 (1991).
[7] S. J. Singer, K. F. Freed, and Y. B. Band, Chem. Phys. Lett. **105**, 158 (1984).
[8] C. J. Williams and K. F. Freed, J. Chem. Phys. **85**, 2699 (1986).
[9] E. Tiemann, H. Kanamori, and E. Hirota, J. Chem. Phys. **88**, 2457 (1988).
[10] Y. Matsumi, P. K. Das, and M. Kawasaki, J. Chem. Phys. **92**, 1696 (1990).
[11] Y. Matsumi, K. Tonokura, M. Kawasaki, and T. Ibuki, J. Chem. Phys. **93**, 7981 (1990).
[12] J. Park, Y. Lee, and G. W. Flynn, Chem. Phys. Lett. **186**, 441 (1991); **192**, 138 (1992) (erratum).
[13] Y. Matsumi, P. K. Das, M. Kawasaki, K. Tonokura, T. Ibuki, G. Inoue, S. Satyapal, and R. Bersohn, J. Chem. Phys. **97**, 5261 (1992).
[14] D. E. Manolopoulos and M. H. Alexander, J. Chem. Phys. **97**, 2527 (1992).
[15] M. H. Alexander, C. Rist, and D. E. Manolopoulos, J. Chem. Phys. **97**, 4836 (1992).
[16] M. H. Alexander, Comput. Phys. Commun. **75**, 87 (1993).
[17] Y. B. Band, K. F. Freed, and D. J. Kouri, J. Chem. Phys. **74**, 4380 (1981).
[18] E. C. Y. Inn, J. Atmos. Sci. **32**, 2375 (1975).
[19] D. E. Manolopoulos, Ph.D. thesis, University of Cambridge, 1988.
[20] B. R. Johnson, J. Comput. Phys. **13**, 445 (1973).
[21] F. Mrugala and D. Secrest, J. Chem. Phys. **78**, 5954 (1983).
[22] F. Mrugala and D. Secrest, J. Chem. Phys. **79**, 5960 (1983).
[23] F. Mrugala, J. Comput. Phys. **58**, 113 (1985).
[24] M. Shapiro and R. Bersohn, Annu. Rev. Phys. Chem. **33**, 409 (1982).
[25] J. T. Hougen, Natl. Bur. Stand. (U.S.) Monograph **115** (1970).
[26] D. L. Albritton, W. J. Harrop, A. L. Schmeltekopf, and R. N. Zare, J. Mol. Spectrosc. **46**, 37 (1973).
[27] H. Lefebvre-Brion and R. W. Field, *Perturbations in the Spectra of Diatomic Molecules* (Academic, New York, 1986).
[28] J. M. Brown, J. T. Hougen, K.-P. Huber, J. W. C. Johns, I. Kopp, H. Lefebvre-Brion, A. J. Merer, D. A. Ramsay, J. Rostas, and R. N. Zare, J. Mol. Spectrosc. **55**, 500 (1975).
[29] C. E. Moore, *Atomic Energy Levels* (NSRDS-NBS 35, U.S. Government Printing Office, Washington, D.C., 1971).
[30] F. H. Mies, Phys. Rev. A **7**, 942 (1973).
[31] V. Aquilanti and G. Grossi, J. Chem. Phys. **73**, 1165 (1980).
[32] V. Aquilanti, P. Casavecchia, G. Grossi, and A. Laganá, J. Chem. Phys. **73**, 1173 (1980).
[33] M. H. Alexander and B. Pouilly, in *Selectivity in Chemical Reactions*, edited by J. C. Whitehead (Kluwer, Drodrecht, 1988), p. 265.
[34] S. J. Singer, K. F. Freed, and Y. B. Band, J. Chem. Phys. **77**, 1942 (1982).
[35] D. M. Hirst and M. F. Guest, Mol. Phys. **41**, 1483 (1980).
[36] M. Bettendorf, S. D. Peyerimhoff, and R. J. Buenker, Chem. Phys. **66**, 261 (1982).
[37] R. A. Kendall, T. H. Dunning, Jr., and R. J. Harrison, J. Chem. Phys. **96**, 6796 (1992).
[38] D. E. Woon and T. H. Dunning, Jr., J. Chem. Phys. **98**, 1358 (1992).
[39] P. J. Knowles and H.-J. Werner, Chem. Phys. Lett. **115**, 259 (1985).

[40] R. N. Diffenderfer and D. R. Yarkony, J. Phys. Chem. **86**, 5098 (1982).
[41] B. H. Lengsfield, J. Chem. Phys. **77**, 4073 (1982).
[42] H.-J. Werner and W. Meyer, J. Chem. Phys. **74**, 5794 (1981).
[43] H.-J. Werner and P. J. Knowles, J. Chem. Phys. **89**, 5803 (1988).
[44] R. J. Gadnitz and R. Alrichs, Chem. Phys. Lett. **143**, 413 (1988).
[45] MOLPRO is a package of *ab initio* programs written by H.-J. Werner and P. J. Knowles, with contributions from J. Almlöf, R. Amos, S. Elbert, W. Meyer, E. A. Reinsch, R. Pitzer, and A. Stone.
[46] S. F. Boys and F. Benardi, Mol. Phys. **19**, 553 (1970).
[47] E. R. Davidson and D. W. Silver, Chem. Phys. Lett. **53**, 403 (1977).
[48] K. P. Huber and G. Herzberg, *Molecular Spectra and Molecular Structure. IV. Constants of Diatomic Molecules* (Van Nostrand–Reinhold, New York, 1979).
[49] J. R. Ogilvie, Proc. R. Soc. London Ser. A **378**, 287 (1981).
[50] E. E. Whiting, A. Schadee, J. B. Tatum, J. T. Hougen, and R. W. Nicholls, J. Mol. Spectrosc. **80**, 249 (1980).
[51] Tables of these matrix elements, as well as a FORTRAN program to determine these, and the four HCl potential energy curves, as a function of R is available on request from the authors by electronic mail (address: mha@hibridon.umd.edu or pouilly@lsm350.citilille.fr). Please supply a return electronic mail address.
[52] A. Untch, K. Weide, and R. Schinke, J. Chem. Phys. **95**, 6496 (1991).
[53] C. Rist and M. H. Alexander, J. Chem. Phys. **98**, 6196 (1993).
[54] HIBRIDON is a package of programs for the time-independent quantum treatment of inelastic collisions and photodissociation written by M. H. Alexander, D. E. Manolopoulos, H.-J. Werner, and B. Follmeg, with contributions by P. F. Vohralik, D. Lemoine, G. Corey, B. Johnson, T. Orlikowski, W. Kearney, A. Berning, A. Degli-Esposti, C. Rist, and P. Dagdigian.
[55] M. H. Alexander, J. Chem. Phys. **76**, 429 (1982).
[56] E. F. van Dishoeck and A. Dalgarno, J. Chem. Phys. **79**, 873 (1983).
[57] E. F. van Dishoeck, J. Chem. Phys. **86**, 196 (1987).
[58] R. N. Zare, *Angular Momentum* (Wiley, New York, 1988).
[59] In Ref. 4, the expression for the photodissociation cross section is *missing* the rotational line-strength factor of 2/3 discussed in Sec. V. Since this factor is routinely present in publications from the same group (Refs. 56 and 57), we here assume that it was included in the calculations, but inadvertently omitted from the publication.
[60] J. F. Ogilvie and D. Koo, J. Mol. Spectrosc. **61**, 332 (1976).